REPORT DOCUMENTATION PAGE

Form Approved
OMB No. 0704-0188

1. REPORT DATE	2. REPORT TYPE	3. DATES COVERED *(From - To)*
07 December 2017	Journal Article	24 February 2017 - 31 December 2017

4. TITLE AND SUBTITLE
Direct Simulation Monte Carlo Application of the Three-Dimensional Forced Harmonic Oscillator Model

5a. CONTRACT NUMBER

5b. GRANT NUMBER

5c. PROGRAM ELEMENT NUMBER

6. AUTHOR(S)
S. Gimelshein, I. Wysong, I. Adamovich

5d. PROJECT NUMBER

5e. TASK NUMBER

5f. WORK UNIT NUMBER
Q1MK

7. PERFORMING ORGANIZATION NAME(S) AND ADDRESS(ES)
Air Force Research Laboratory (AFMC)
AFRL/RQRC
10 E. Saturn Blvd.
Edwards AFB, CA 93524-7680

8. PERFORMING ORGANIZATION REPORT NUMBER

9. SPONSORING/MONITORING AGENCY NAME(S) AND ADDRESS(ES)
Air Force Research Laboratory (AFMC)
AFRL/RQR
5 Pollux Drive
Edwards AFB, CA 93524-7048

10. SPONSOR/MONITOR'S ACRONYM(S)

11. SPONSOR/MONITOR'S REPORT NUMBER(S)
AFRL-RQ-ED-JA-2017-043

12. DISTRIBUTION/AVAILABILITY STATEMENT
Approved for Public Release; Distribution Unlimited. PA Clearance Number: 17160 Clearance Date: 31 March 2017

13. SUPPLEMENTARY NOTES
Journal article published in the Journal of Thermophysics and Heat Transfer, Articles in Advance; DOI: 10.2514/1.T5228
Publication Date (Web): 07 December 2017;
Prepared in collaboration with ERC and Ohio State University

14. ABSTRACT
An implementation of the three-dimensional forced harmonic oscillator model of vibration–translation energy transfer in atom–diatom and diatom–diatom collisions is proposed. The implementation employs precalculated lookup tables for transition probabilities and is suitable for the direct simulation Monte Carlo method. It takes into account the microscopic reversibility between the excitation and deexcitation processes, and it satisfies the detailed balance requirement at equilibrium. The implementation is verified for oxygen and nitrogen thermal heat baths and validated for aftershock relaxation of oxygen in argon. Comparison with the one-dimensional forced harmonic oscillator model shows large differences in macroparameters for high-temperature bath relaxation and moderate-tolarge differences in realistic oxygen shock conditions.

15. SUBJECT TERMS

16. SECURITY CLASSIFICATION OF:			17. LIMITATION OF ABSTRACT	18. NUMBER OF PAGES	19a. NAME OF RESPONSIBLE PERSON
a. REPORT	b. ABSTRACT	c. THIS PAGE			Ingrid Wysong
Unclassified	Unclassified	Unclassified	SAR	11	19b. TELEPHONE NUMBER *(Include area code)* N/A

Direct Simulation Monte Carlo Application of the Three-Dimensional Forced Harmonic Oscillator Model

Sergey F. Gimelshein*
ERC, Inc., Edwards Air Force Base, California 93524
Ingrid J. Wysong†
Air Force Research Laboratory, Edwards Air Force Base, California 93524
and
Igor V. Adamovich‡
The Ohio State University, Columbus, Ohio 43210

DOI: 10.2514/1.T5228

An implementation of the three-dimensional forced harmonic oscillator model of vibration–translation energy transfer in atom–diatom and diatom–diatom collisions is proposed. The implementation employs precalculated lookup tables for transition probabilities and is suitable for the direct simulation Monte Carlo method. It takes into account the microscopic reversibility between the excitation and deexcitation processes, and it satisfies the detailed balance requirement at equilibrium. The implementation is verified for oxygen and nitrogen thermal heat baths and validated for aftershock relaxation of oxygen in argon. Comparison with the one-dimensional forced harmonic oscillator model shows large differences in macroparameters for high-temperature bath relaxation and moderate-to-large differences in realistic oxygen shock conditions.

I. Introduction

MODELING of high-temperature nonequilibrium air flows is traditionally complicated by significant uncertainties associated with various aspects of high-energy molecular interactions. One of the key aspects of these interactions is the energy transfer between the translational and internal–rotational and vibrational modes of the colliding molecules [1,2]. The rotational mode is characterized by small energy gaps between energy levels, and thus, in most cases of interest, may be fairly accurately described by a continuous-energy model. In this case, a single temperature- or energy-dependent rotational relaxation rate governs the energy exchange. The vibrational mode does not provide such convenience because large energy gaps between levels, especially in the lower part of the spectrum, require the comprehensive computational model to consider these levels separately. Neglecting the discrete energy structure of the vibrational mode is expected to significantly affect the translation–rotation–vibration energy transfer and the dissociation and exchange reaction rates. This, in turn, may result in an unacceptable error in predicting the radiation signatures from IR to UV, as well as the heat fluxes to the wall.

Consideration of the discrete structure of the vibrational mode inherently implies the definition of the key energy transfer paths to and from the vibrational level. In the most general case, that means one needs to specify the cross sections:

$$\sigma\left(v_1, v_2, J_1, J_2, E_t \rightarrow v_1', v_2', J_1', J_2', E_t'\right) \tag{1}$$

the corresponding energy dependent transition probability P, or the translational–rotational temperature-dependent rate k. Here, v and J are the vibrational and rotational levels of colliding molecules 1 and 2, E_t is the relative translational energy, and symbols $'$ denote the postcollisional states. The cross sections in the form of Eq. (1) may be obtained using different ab initio approaches, such as quasi-classical scattering theory [3,4] or trajectory [5] calculations, semiclassical, as well as close-coupled [6,7] or full [8] quantum mechanical approaches. In recent years, there has been significant effort aimed at better understanding of the thermal processes of air species, and much recent work has examined internal energy excitation at detailed state-to-state trajectory calculations and the direct molecular dynamics level. Examples are [9,10] for N_2–N_2 collisions, [11,12] for N_2–N, and [13,14] for O_2–O.

The use of complete transition cross sections [Eq. (1)] has some obvious practical complications. Because the complete transition matrix for the collision of two diatomic molecules, such as N_2–N_2, includes on the order of 10^{18} elements, its precomputed tabulated representation and use in flow simulations is not possible in the foreseeable future. An alternative to the precomputed tables is the direct on-the-fly calculation of transition cross sections during the flow simulation. The concept, recently introduced for particle simulations in [15,10] and called direct molecular simulation (DMS), combines the direct simulation Monte Carlo (DSMC) method for rarefied gas flows and the quasi-classical trajectory (QCT) calculations approach for ab initio modeling of collision processes. The DMS method builds on an earlier work [16,17], improving the latter with more accurate modeling of the collision process.

Accurate ab initio modeling of the collisional process in the DSMC method allows detailed analysis of the gas relaxation in spatially homogeneous or one-dimensional flows, but it becomes prohibitively time consuming for multidimensional problems, especially in the near-continuum flow regime. An alternative is to simplify the transition probability in the first approximation, presenting it [18] as the product of the vibration–translation (VT) and rotation–translation (RT) transition probabilities. In this case, the RT process may be modeled separately using the Jeans relaxation equation and a temperature-dependent RT relaxation rate in the solution of the Navier-Stokes equations, or its equivalent based on the Larsen–Borgnakke [19] approach in the DSMC method. For the VT relaxation, several techniques may be used that differ in their accuracy and complexity; those applicable to the DSMC method are listed in the following.

The simplest and most widely used, but possibly least accurate, is the technique based on the discrete Larsen–Borgnakke model [20] of local-equilibrium energy redistribution, with a temperature-dependent vibrational relaxation number $Z_v(T)$ often defined from the vibrational relaxation time [21]. This model captures the VT energy transfer process but neglects the vibration–vibration (VV) process. An approach with much greater accuracy and complexity is

Received 31 March 2017; revision received 3 November 2017; accepted for publication 5 November 2017; published online 7 December 2017.

*Aerospace Engineer.
†Technical Advisor, Combustion Devices Branch.
‡Professor, Department of Mechanical Engineering.

to directly use quasi-classical or quantum mechanic calculations. Such models do not attempt to perform on-the-fly ab initio calculations but use precalculated VT and/or VV tables. One of the earlier examples here is the work of [22], where the quasi-classical theory was used to precalculate separate VT and resonant VV transition tables and then use them in subsequent DSMC simulations. The drawbacks of this approach were the limited range of temperatures that it captured [23] and the lack of accuracy in collisions that included nitrogen or oxygen atoms. One can also use the transition data obtained in recent QCT computations [9–14], although the limiting factor may be the shear amount of information that needs to be stored and used in the modeling of reacting air. Due to this limitation, an alternative approach is currently under development that aims at reducing the prohibitively large number of level-by-level transitions to a set manageable from the computer implementation perspective [24].

Between the two limits (the fully empirical and the ab initio quasi-classical and quantum mechanic approaches), there are approaches that use some assumptions and approximations to provide general expressions for the VT transition probabilities. Most of those may be classified into one of the two groups: the first-order perturbation theory (FOPT) methods [25] and methods based on the nonperturbative semiclassical forced harmonic oscillator (FHO) theory [26,27]. The FOPT methods neglect a sequential mechanism of single-quantum transition steps in a single collision, and they are known to underpredict semiclassical calculations by orders of magnitude [18]. On the other hand, the FHO theory, based on that sequential mechanism, was shown to provide very good agreement with such calculations [18]. Although previous studies of nonequilibrium flows have included FHO expressions for resonant VV exchanges, comparison cases for a single-species gases both with and without a resonant VV process show, not surprisingly, little effect (see, for example, [22]). On the contrary, nonresonant VV exchanges in interspecies molecule–molecule collisions is known to be an important effect in changing the overall vibrational relaxation time: for instance, in nitrogen–oxygen mixtures [28]. Although the FHO theory does include derivations for nonresonant exchanges, the actual numerical implementation presents nearly unsurmountable challenges due to prohibitively large transition tables for a precomputed calculation of transition probabilities and excessively complex probability expressions for on-the-fly probability calculation during the flow simulation.

The first self-consistent FHO model suitable for particle simulations was developed in [29], where a one-dimensional FHO approach was used for atom–diatom and diatom–diatom collisions, with a steric factor introduced to match the semiclassical results [6] at lower energies. The steric factors were necessary to compensate for the dependence of transition probabilities on the orientation of the colliding partners that was not taken into account in the one-dimensional FHO model. The model [29] was implemented and used in a number of recent studies [30–34]. Note also that the FHO approach is fairly similar to the model [16,17], where the simple harmonic oscillator model was used with FHO VT and VV transitions (only one-quantum resonant transitions were modeled for VV). Note, however, that the use of adjustable parameters such as "steric factors" often masks the lack of understanding of collision dynamics, as was shown in more recent studies of vibrational energy transfer in three-dimensional atom–molecule and molecule–molecule collisions [35,36]. In particular, it was shown that modulation of interaction potential by molecular rotation during collisions may increase vibrational energy transfer probability so significantly that the steric factor would have to exceed unity. This illustrates a major flaw of this semiempirical approach. Significant improvements have been made in the FHO formalism by introducing a free-rotation (FR) FHO (FHO-FR) model [35,36], where the full three-dimensional dynamics of collisions between a rotating diatomic molecule and an atom or another diatomic molecule was considered. Because full three-dimensional (3-D) collisions are considered, there is no need for adjustable parameters such as steric factors in the FHO-FR model.

Although potentially more accurate, especially at higher temperatures, the FHO-FR model has not yet been used in the DSMC method. Its implementation may, however, provide significant benefits, as will be shown in the following through the comparison with experimental data on atomic oxygen recombination. The main objectives of this work are therefore to present an implementation of the VT FHO-FR model in particle simulations that enforces the detailed balance at equilibrium and provides good agreement with measured VT transition rates, as well as to examine the impact of the 3-D free-rotation mechanism in hypersonic flows. The FHO theory is adapted to the DSMC method only for VT energy exchanges due to computational challenges of implementing the full array of VV transitions mentioned earlier. Note here that an account of VV processes is not expected to influence the results presented in the following because they are most pronounced in flows where there are at least two molecular species with significantly different VT relaxation rates, such as air, which are not considered in this work.

II. FHO-FR Model for the DSMC Method

The FHO-FR [35,36] is a three-dimensional nonperturbative, semiclassical analytic model of vibrational energy transfer in collisions between a rotating diatomic molecule and an atom, as well as between two rotating diatomic molecules. In its most general form [18], it incorporates rotational relaxation and coupling between vibrational, translational, and rotational energy transfer. An analysis of semiclassical trajectories of rotating molecules interacting by a repulsive exponential atom-to-atom potential resulted in closed-form analytic expressions of VT and VV transition probabilities as functions of rotational and relative translational energies of colliding particles. Such an energy dependence makes the model suitable for the DSMC method, and the specific implementation proposed for the VT energy exchange is outlined in this section.

The probability of a VT transition of a diatomic molecule from its precollisional vibrational level i to its postcollisional level f in a collision with an atom may be written as [35]

$$P(i\to f|E,\epsilon,y,\vartheta,\phi)=\frac{(n_s)^s}{(s!)^2}Q^s\exp\left\{-\frac{2n_s}{s+1}Q-\frac{n_s^2}{(s+1)^2(s+2)}Q^2\right\} \tag{2}$$

where

$$s=|i-f|,\quad n_s=\left(\frac{\max(i,f)!}{\min(i,f)!}\right)^{1/s},$$

$$Q\equiv Q(u,\epsilon,y,\vartheta,\phi)=\frac{\theta'\xi\cos^2\vartheta\cos^2\phi}{4\theta\sinh^2(\pi\omega/\alpha u\gamma)}$$

In the preceding expression, θ is the characteristic vibrational temperature,

$$\omega=\frac{|E_{\mathrm{vib},i}-E_{\mathrm{vib},f}|}{s\hbar}$$

is the average vibrational quantum for the transition $i\to f$; $\epsilon=E_{\mathrm{rot}}/E$ is the fraction of the rotational energy E_{rot} in the translation–rotation energy $E=E_{\mathrm{rot}}+E_{\mathrm{tr}}$; $2\xi=(m/m_o)$ is the ratio of the collision reduced mass m to the oscillator reduced mass m_o; α is the Morse potential interaction parameter; ϑ and ϕ are the orientation angles of the molecule;

$$\theta'=\frac{4\pi^2\omega^2 m}{\alpha^2 k}$$

$u\gamma$ is the effective collision velocity, with $u=\sqrt{2E/m}$ and

$$\gamma=\max\left(0,-0.5\sin(2\vartheta)\cos(\phi)\sqrt{\xi\epsilon}+\sqrt{(1-\epsilon)(1-y)}\right)$$

and $y=(b/R_0)^2$ is the squared ratio of the impact parameter b to the collision diameter R_0.

It is important to note that, for $\epsilon = y = \vartheta = \phi = 0$, the FHO-FR model reduces to the one-dimensional FHO model [29].

There are generally two possible ways to implement the above VT probabilities into the DSMC method. First, one can directly calculate the probabilities for every atom–diatom collision, based on their relative translational and rotational energies and randomly choosing the orientation angles ϑ and ϕ that are uniformly distributed between zero and 2π, as well a parameter y uniformly distributed between zero and one. Such an approach requires a three-step procedure:

1) Calculate the total probability of the VT transition as the sum

$$P_{\text{sum}}(\epsilon, u) = \sum_f P(i \to f|\epsilon, u)$$

over all allowed vibrational states f (either the ground level for deexcitation and maximum vibrational level for the given E_{tr} or bounded by some preset maximum vibrational jumps).

2) Accept VT transition with the probability P_{sum}.

3) Determine the postcollision vibrational state f according to the probability $P(i \to f)/P_{\text{sum}}$.

Step 1, which is the determination of all possible transition probabilities for every collision, is fairly time consuming and is expected to increase the computational time typically required for the collision step of the DSMC method by approximately five times. Because the collision step usually takes up to 30% and, for many near continuum cases, up to 70% of the total computational time, this approach involves significant computational overhead.

An alternative approach, used in this work and similar in implementation to that of [22], is to apply precomputed lookup tables. In this case, the probabilities P_{sum} and $P(i \to f)/P_{\text{sum}}$ are precalculated, and the flow simulation requires only steps 2 and 3, with negligible computational overhead added as compared to the on-the-fly approach (that overhead is, in fact, even smaller than for the conventional Larsen–Borgnakke procedure). The lookup tables are calculated through the Monte Carlo integration that, for the deexcitation process of $f < i$, may be presented as the following sum:

$$P_{i>f}(i \to f|E) = \frac{1}{M}\sum_{m=1}^{M} P_{m,i>f}(i \to f|E, \epsilon_m, y_m, \vartheta_m, \phi_m) \quad (3)$$

Here, M is the sampling size of the Monte Carlo integration (on the order of 10^6 in this work).

It is important to note that, in the present implementation, the transition probabilities in the lookup tables are the functions of the translation–rotation energy E but not the fraction of the rotational energy ϵ, with the latter included in the integration. Such an approach is necessary to greatly reduce the lookup table, and thus the corresponding computer array size, from about a gigabyte to only a few megabytes for every collision type. The lookup table is therefore constructed for a fixed number of bins N_b of the translation–rotation energy E (on the order of 500). The logarithmic scale is used to define the boundaries of the energy bins, with the upper boundary of the n_bth bin, E_{nb}, set as

$$E_{nb} = E_{\min}\left(\frac{E_{\max}}{E_{\min}}\right)^{(n_b-1)/(N_b-1)}$$

To strictly satisfy the detailed balance requirement at equilibrium, the Monte Carlo integration uses the Larsen–Borgnakke-type equipartition assumption to sample the fraction of rotational energy. In this case, ϵ_m is sampled from the probability density $f(\epsilon) = (1-\epsilon)^{1-\eta}$ through an acceptance–rejection procedure with $\epsilon_m = \Re_1$, where $\Re_1$ satisfies the requirement $\Re_2 < (1-\Re_1)^{1-\eta}$. Here, $\Re_1$ and $\Re_2$ are the random numbers uniformly distributed between zero and one, and η is the exponent in the variable hard sphere (VHS)/variable soft sphere (VSS) [1,37] interaction models ($\eta = 0$ for hard spheres, and $\eta = 0.5$ for Maxwell molecules).

The impact and orientation parameters are selected as

$$y_m = \Re, \qquad \vartheta_m = 2\pi\Re, \qquad \phi_m = 2\pi\Re$$

Here, $\Re$ again denotes random numbers uniformly distributed between zero and one. After the values of ϵ_m, y_m, ϑ_m, and ϕ_m are sampled according to the aforementioned procedure for every m, the mth transition probability

$$P_{m,i>f}(i \to f|E, \epsilon_m, y_m, \vartheta_m, \phi_m)$$

is calculated from Eq. (2), and then it contributes to the summation in Eq. (3).

The excitation probability table is also constructed through Monte Carlo integration, with the summation similar to Eq. (3):

$$P_{i<f}(i \to f|E) = \frac{1}{M'}\sum_{m=1}^{M} P_{m,i<f}(i \to f|E, \epsilon_m, y_m, \vartheta_m, \phi_m) \quad (4)$$

Note here that, in the excitation process, there are summation points m for which the translational energy is not large enough to overcome the vibrational energy gap $E_{\text{vib},f} - E_{\text{vib},i}$. Clearly, the VT transition probability for such collisions is zero, and they should not be considered in the summation. M' is, therefore, the number of sampling points with $E > E_{\text{vib},f} - E_{\text{vib},i}$. Similar to the deexcitation process, the excitation probabilities $P_{m,i<f}$ are calculated for N_b translation–rotation energy bins. The values of ϵ_m, y_m, ϑ_m, and ϕ_m are also sampled according the deexcitation scheme. Then, the probability $P_{m,i<f}$ is calculated from the microscopic reversibility condition:

$$g_i^2\sigma(i, g_i \to f, g_f) = g_f^2\sigma(f, g_f \to i, g_i) \quad (5)$$

where i, g_i and f, g_f are the vibrational state and relative collision energy pre- and postcollision, respectively. From Eq. (5), and recalling that the postcollision translational energy is

$$E_{\text{tr},f} = (1-\epsilon_m)E + E_{\text{vib},i} - E_{\text{vib},f}$$

one can express the excitation probability for the VHS/VSS interaction model through the corresponding deexcitation probability as

$$P_{m,i<f}(i \to f|E, \epsilon_m, y_m, \vartheta_m, \phi_m) = \left(\frac{g_f}{g_i}\right)^{2-2\eta} P_{m,i>f}(i \to f|E'_m\epsilon'_m, y_m, \vartheta_m, \phi_m) \quad (6)$$

where

$$E' = E_{\text{tr},f} + \epsilon_m E, \;\; \epsilon'_m = \frac{\epsilon_m E}{E'}, \;\; g_i = \sqrt{\frac{2(1-\epsilon_m)E}{m}}, \;\; g_f = \sqrt{\frac{2E_{\text{tr},f}}{m}}$$

Consider now the collision of two diatomic molecules. In this case, the FHO-FR probabilities of a VT transition in one of the colliding molecules may also be written [36] through Eq. (2); although, in this case,

$$Q(u, \epsilon, y, \vartheta, \phi) = \frac{\theta'\xi\cos^2\vartheta_1\cos^2\phi_1}{4\theta\sinh^2(\pi\omega_1/\alpha u\gamma)}$$

and

$$\gamma = \max\Big(0, -0.5\sin(2\vartheta_1)\cos(\phi_1)\sqrt{\epsilon_1} - 0.5\sin(2\vartheta_2)\cos(\phi_2)\sqrt{\epsilon_2} + \sqrt{(1-\epsilon_1-\epsilon_2)(1-y)}\Big)$$

Here, subscripts 1 and 2 refer to the molecule changing its vibrational state and its colliding partner, respectively. The FHO-FR reduces to the one-dimensional FHO model when

$$\epsilon_1 = \epsilon_2 = y = \vartheta_1 = \vartheta_2 = \phi_1 = \phi_2 = 0$$

The VT probabilities are again calculated for N_b translation–rotation energy bins E_{nb}, although the energy E is now $E = E_{\text{tr}} + E_{\text{rot},1} + E_{\text{rot},2}$. The Monte Carlo integration procedure for the deexcitation process may be written as

$$P_{i>f}(i \to f|E) = \frac{1}{M}\sum_{m=1}^{M} P_{m,i>f}(i \to f|E, \epsilon_{m,1}, \epsilon_{m,2}, y_m, \vartheta_{m,1}, \vartheta_{m,2}, \phi_{m,1}, \phi_{m,2}) \quad (7)$$

The fractions of rotational energy of the first and second molecules $\epsilon_{m,1}$ and $\epsilon_{m,2}$ for each m are found as follows. First, the sum $\epsilon_{m,12} = \epsilon_{m,1} + \epsilon_{m,2}$ is sampled from the probability density $f(\epsilon_{12}) = \epsilon_{12}(1-\epsilon_{12})^{1-\eta}$ through an acceptance–rejection procedure with $\epsilon_{m,12} = \Re_1$, where $\Re_1$ satisfies the requirement $\Re_2 < \Re_1(1-\Re_1)^{1-\eta}/F_m$. Here,

$$F_m = x_m(1-x_m)^{1-\eta}, \quad x_m = \frac{1}{2-\eta}$$

After that, $\epsilon_{m,1}$ and $\epsilon_{m,2}$ are found as $\epsilon_{m,1} = \epsilon_{12}\Re$ and $\epsilon_{m,2} = \epsilon_{12} - \epsilon_{m,1}$.

The impact and orientation parameters are obtained through

$$y_m = \Re, \ \vartheta_{m,1} = 2\pi\Re, \ \vartheta_{m,2} = 2\pi\Re, \quad \phi_{m,1} = 2\pi\Re \ \phi_{m,2} = 2\pi\Re$$

The excitation VT probability for diatom–diatom collisions may be calculated similar to Eq. (6); but, in this case,

$$E_{\text{tr},f} = (1-\epsilon_{m,12})E + E_{\text{vib},i} - E_{\text{vib},f}, \quad E' = E_{\text{tr},f} + \epsilon_{m,12}E$$
$$\epsilon'_{m,1} = \frac{\epsilon_{m,1}E}{E'}, \quad \epsilon'_{m,2} = \frac{\epsilon_{m,2}E}{E'}, \quad \epsilon'_{m,12} = \frac{\epsilon_{m,12}E}{E'},$$
$$g_i = \sqrt{\frac{2(1-\epsilon_{m,12})E}{m}}, \quad g_f = \sqrt{\frac{2E_{\text{tr},f}}{m}}$$

For both atom–diatom and diatom–diatom collisions, the excitation and deexcitation probabilities are calculated for a vibrational jump s varying from zero to the maximum allowable jump $s_{\max}$. Hereafter, $s_{\max}$ is set to 10 because using larger numbers was found to have negligible effect on the results (see also [38]). For every i, the overall probability P_{sum} and the probability ratios $P(i \to f)/P_{\text{sum}}$ are calculated and then used in the DSMC modeling.

As noted earlier, the FHO-FR model does not have any adjustable parameters, providing the energy-dependent VT probabilities only as functions of physical properties, such as Morse and oscillator parameters, for any colliding atom–molecule and molecule–molecule species pair. The model also uses prescribed values of the total collision cross sections, which are typically set at about 40 Å^2 for atom–diatom and 60 Å^2 for diatom–diatom collisions [36] because those values are found to provide excellent agreement with three-dimensional semiclassical trajectory calculations. In the DSMC method, however, the direct use of FHO-FR probabilities implies that these probabilities will be applied in conjunction with the DSMC-specific total collision cross sections: usually those of the VHS/VSS models. Note that both VHS and VSS collisions may be considered "strong" as compared to more realistic potentials such as the Lennard–Jones or inverse-power law, in a sense that both the VHS and VSS are characterized by large after-collision scattering angles, and correspondingly small collision diameters.

Because of the "strong collision" limitation of the VHS and VSS collision models, which use either a hard or soft sphere approximation for the total scattering cross section, the present model needs to use a cross-section adjustment parameter (CAP), which is a scaling factor by which all inelastic energy transfer probabilities are increased to match the cross sections predicted using a more accurate molecular interaction potential. Note that the use of the CAP factor is necessitated by the implementation of the DSMC method (in particular, neglecting collisions with large impact parameters/small scattering angles, which results in underprediction of the total scattering cross section). The CAP factor is therefore a correction related to the total collision cross section and not the vibrational energy transfer model used.

Note also that the use of a more realistic intermolecular potential, such as the Lennard–Jones or the Morse potential, in the DSMC method may not remove the need for a the CAP. This is primarily because practical implementation of any such potential would require the use of a cutoff value of the scattering angle (or the impact parameter), which in turn introduces an arbitrariness in the number of modeled collisions and in the resultant VT rate. The CAP allows for an effective independence of the VT rate in the simulation on such an arbitrariness.

III. Verification Analysis of the FHO-FR Implementation

The first step in the verification process of the proposed implementation of the FHO-FR model is conducted at the microscopic (collision energy) level, and it includes the comparison of the calculated VT transition probabilities with published results [35,36]. The Monte Carlo integration over the rotational energy and the impact and orientation parameters used in the present work to obtain relative collision energy-dependent transition probabilities is generally similar to that of [35,36], with two notable exceptions. The first is purely numerical: the probability sampling was conducted here over 640,000 random trajectories m, and not 1000. The statistical error bar is therefore less than 1%, as compared to over 10% of [35,36]. The second distinction is physical and related to the selection of the rotational fractions ϵ for atom–diatom and ϵ_1 and ϵ_2 for diatom–diatom collisions. The present implementation uses a Larsen–Borgnakke-type approach that allows one to strictly satisfy the detailed balance requirement in equilibrium gas. The work [35,36] has used the uniform selection of the rotational fractions, for consistency with the trajectory calculations [6]. For atom–diatom collisions, the difference is fairly small, and it becomes nonexistent for a hard sphere collision model. For molecule–molecule collisions, the difference is more significant.

Consider diatom–atom collisions of an N_2 molecule with an atom of the same mass. The transition probabilities for two single-quantum and two multiquantum deexcitation jumps are plotted in Fig. 1 (left). The present FHO-FR implementation is compared here with the FHO-FR results of [35] and with the trajectory calculations results [35] obtained using the ADIAV computer code [6]. There is generally very good agreement between the two FHO-FR implementations: both of which are also within a factor of two from the trajectory calculation results. The agreement is not as good, but is still acceptable, for N_2–N_2 collision probabilities, shown in Fig. 1 (right). In this case, the present implementation is still within approximately a factor of two from either the FHO-FR [36] or DIDIEX computer code [6]. Note that the agreement is clearly better for single-quantum deexcitation probabilities than for multiquantum ones. Part of the reason for the observed differences lies in the different selection method of the rotational energy fractions, as the work in [36] has indicated strong dependence of transition probabilities on both ϵ_1 and ϵ_2.

The next step in model verification is the check of the detailed balance condition. In equilibrium gas, the microscopic reversibility for the forward and reverse transition probabilities between different states results in the detailed balance of temperature-dependent rates of different processes [39]. The implication here is that all mode temperatures (translational, rotational, and vibrational) should be equal at equilibrium; moreover, gas initially at a nonequilibrium should reach equilibrium through collisional relaxation. At the microscopic level, the energy distributions should be Boltzmann in equilibrium gas. To verify that the equilibrium condition is maintained, and nonequilibrium gas relaxes to equilibrium, both isothermal and adiabatic spatially homogeneous baths are examined for different gas mixtures of Ar, O_2, and N_2, with equilibrium

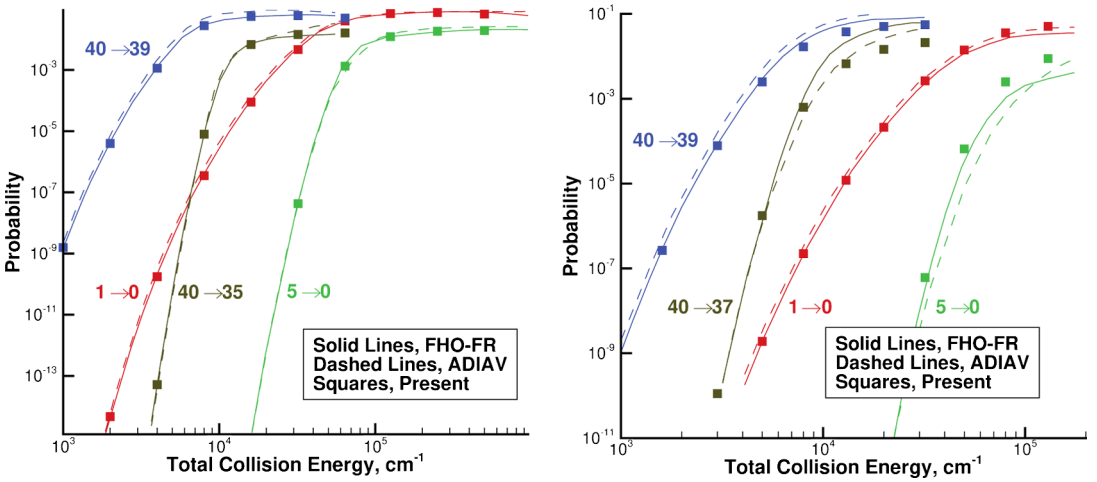

Fig. 1 Deexcitation probabilities for atom–diatom (left) and molecule–molecule (right) collisions.

temperatures ranging from 4000 to 20,000 K. The SMILE DSMC code [40], which is extended to include the FHO-FR lookup tables, is used in all computations.

Examples of the relaxation of molecular nitrogen from initially equilibrium and nonequilibrium states are presented in Fig. 2 (left). For the former case, the gas was initially at full equilibrium at a temperature of 10,000 K and a number density of 10^{26} molecule/m^3. The temporal relaxation was recorded for 2000 mean collision times. The result, shown by nearly flat translation–rotation–vibration temperatures at 10,000 K, indicated that the vibrational temperature deviated from its initial value by no more than 0.2%, which was somewhat above the statistical error bars of approximately 0.1%. The deviation was fully attributed to the binning of the relative translational energy space. When the currently used number of bins (500) was increased to 2000, the vibrational temperature was within the statistical error bars from its initial value. The accuracy of 0.2% was still quite acceptable in most cases, and thus the number of energy bins of 500 could be recommended for general use.

The nonequilibrium relaxation case shown in Fig. 2 (left) is conducted for the initial $T_{tr} = T_{rot} = 15{,}000$ K and $T_{vib} = 300$ K. As illustrated in the figure, all mode temperatures converge to their equilibrium value of about 10,940 K, and they do not deviate from that by more that 15 K. All other tests conducted for different temperatures and gas species show similar agreement of the computed mode temperatures with their equilibrium values. The conclusion therefore may be drawn that the current implementation of the FHO-FR model strictly satisfies the detailed balance requirement at equilibrium. The molecular velocity, rotational and vibrational energy distributions are also checked against the corresponding Maxwell–Boltzmann distribution; the difference between the computed and the analytic distributions is found to be within the statistical error bars. An example of such a comparison is shown in Fig. 2 (right), where the instantaneous vibrational distribution functions are given at a time moment of 20 ns, when the initially nonequilibrium flow of Fig. 2 (left) reaches full equilibrium.

IV. Vibrational Relaxation Time and Model Validation

Although the proposed implementation of the FHO-FR model into the DSMC method provides realistic VT probabilities and maintains the detailed balance at equilibrium, it is also important for the model to capture the temperature dependence of the vibrational relaxation time, for which experimental data and theoretical predictions are available for a wide range of temperatures and many species pairs. As mentioned earlier, the use of the VHS or VSS collision model in the DSMC method makes it necessary to introduce a cross-section adjustment parameter: CAP ≥ 1. Applied to the VT transition probabilities, this parameter takes into account small total collision cross sections of the VHS/VSS models associated with the large-angle postcollision scattering. Note that the VHS/VSS total collision cross section is known to be significantly smaller than those calculated more rigorously. For example, for the N_2–N collisions, the total collision cross section obtained by the QCT method was found [41] to be, on average, about four times larger than that of the VHS or VSS. The actual difference depends on the relative collision energy, and it may be expected to decrease with increasing E_{tr}.

A CAP used in this work attempts to alleviate the cross-section problem. Although one may use a collision energy-dependent CAP, such a dependence unnecessarily complicates the algorithm without significant improvement in accuracy. Because a constant

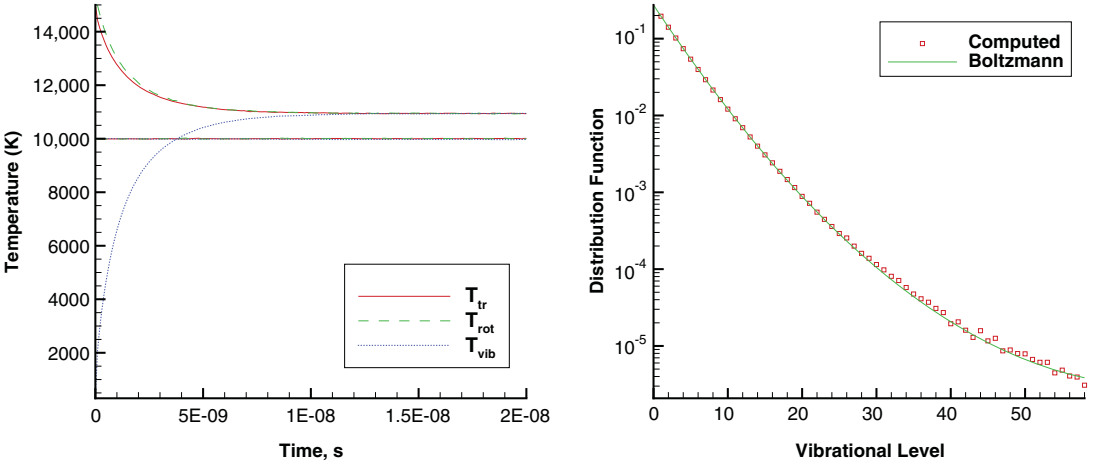

Fig. 2 Relaxation in equilibrium and nonequilibrium nitrogen baths at macroscopic (left) and microscopic (right) levels.

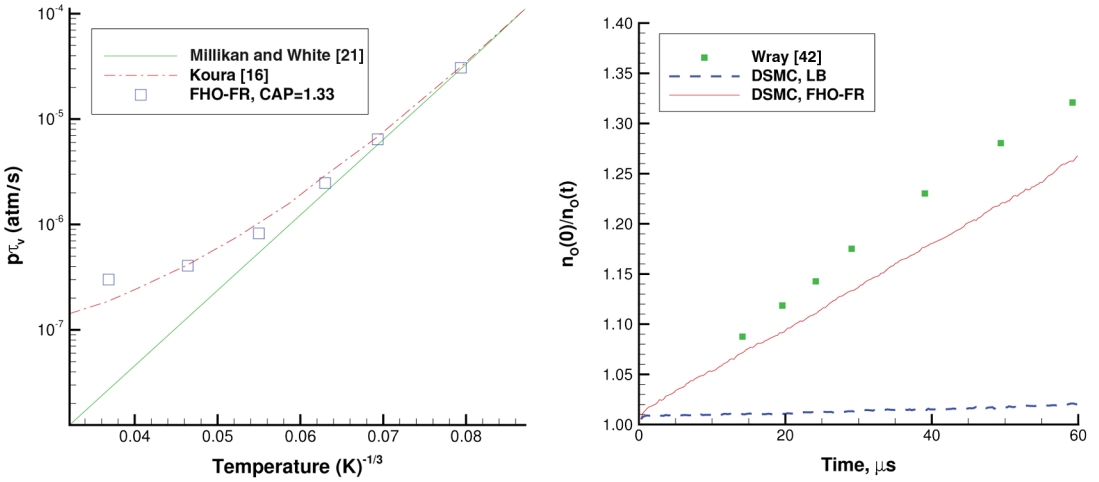

Fig. 3 O_2–Ar thermal bath relaxation: vibrational relaxation time (left) and atomic oxygen concentration (right). Here, LB stands for Larsen-Borgnakke model.

species-pair-dependent CAP is found to provide acceptable (within a factor of two) agreement with temperature-dependent vibrational relaxation time, it is used hereafter. For the O_2–Ar collision pair, a CAP of 1.33 is found to provide good agreement with the Millikan–White semiempirical correlation [21] for gas temperatures up to 8000 K, where the correlation is expected to be applicable. For higher temperatures, the FHO-FR result agrees well with the recommendation [16]. This is illustrated in Fig. 3 (left), which shows the product of the gas pressure p and the vibrational relaxation time τ_v as a function of the gas temperatures.

Although the reasonable behavior of the vibrational relaxation number provides important clues on model performance in conditions close to equilibrium, it is also necessary to validate the model at nonequilibrium conditions, where the vibrational temperature differs significantly from translational and rotational. Such a validation is traditionally difficult for the DSMC method, mostly due to limited availability of experimental data in flow regimes where nonequilibrium effects would be pronounced. In this work, we use ozone pyrolysis experiments [42] where the ozone molecules are quickly transformed to oxygen atoms, which then recombine through collisions with the surrounding gas to produce molecular oxygen. These are shock tube measurements of atomic oxygen concentration as a function of time, where oxygen collisional recombination proceeds in a thermal bath of argon heated to temperatures between 2000 and 3000 K. There is an obvious reason why the experimental data [42] are interesting in terms of vibrational relaxation. Although the oxygen recombination rate is known from the experiment and the after-recombination vibrational states are assigned from detailed balance conditions applicable in a thermal bath conditions of the experiment, and thus relatively well defined, the vibrational relaxation of the very high vibrational levels of molecular oxygen is in fact the largest unknown. Such a relaxation determines the oxygen vibrational level population, and thus the strongly vibrationally favored process of dissociation. The latter, in turn, has direct impact on the computed concentration of atomic oxygen.

The DSMC computation of the thermal bath gas conditions of the shock tube experiments [42] is conducted for a 0.5% O–99.5% Ar mixture initially at 40 cm Hg and 2400 K. Two VT models are used in the computations: the FHO-FR and the discrete Larsen–Borgnakke model. The latter one has a Millikan–White–Park temperature dependence of the vibrational relaxation number close to that of the FHO-FR. The recombination model [43] is used in this work. Comparison of the numerical and experimental results is presented in Fig. 3 (right). The plot shows the temporal relaxation of the ratio of the initial number density of oxygen atoms $n_O(0)$ to the instantaneous time-dependent oxygen atom density $n_O(t)$. The results show that the conventional Larsen–Borgnakke model is unacceptable for this flow because it drastically underpredicts the rate of the recombination process. The reason for this is that the recombination rate is determined by the number of oxygen molecules that populate higher vibrational levels. The VT rate is clearly too low for that model. For the FHO-FR model, on the other hand, there is good agreement: the measured recombination rate is underpredicted by less than 20%.

The FHO-FR model has thus been shown to perform reasonably well in collisions between diatomic molecules and noble gas atoms. Its applicability to collisions of diatomics with nitrogen or oxygen atoms is, however, significantly reduced. The FHO-FR mechanism does not take into account strong attractive forces that dominate such collisions, and it does not include highly possible exchange reactions, which have shown to significantly decrease the VT relaxation time [11]. As a result, it may not reproduce the unconventional temperature dependence of τ_v increasing with the gas temperature at high T, which was established recently for O_2–N collisions [44]. Similar to the one-dimensional (1-D) FHO, discussed in [12], the FHO-FR provides VT rates for N_2–N collisions that are in good agreement with QCT rates for single-quantum VT jumps (not shown here) but significantly differ from them for multiquantum jumps. Therefore, It can be applied to a reduced range of temperatures (likely below 10,000 K, where the multiquantum transitions are of lesser importance), whereas it is not yet clear whether it provides additional accuracy as compared to the Larsen–Borgnakke model with realistic $\tau_v(T)$. Still, the FHO-FR model may be reliably used to model VT energy transfer in collisions of nitrogen and oxygen molecules, as well as these to molecules with nitric oxide. In many cases with interspecies molecule–molecule collisions, VV exchanges will be even more important than the VT relaxation, and a simplified model for VV is currently being developed.

The comparison of the vibrational relaxation time for nitrogen and oxygen gases with several semiempirical and theoretical models is presented in Fig. 4. In this plot, "Millikan and White" refers to semiempirical correlations [21], "Park" [45] and "Boyd" [46]denote the high-temperature corrections of [45,46], and "DMS" is the direct molecular simulation result [10] (available for nitrogen only). The plot shows that the FHO-FR model works well for these collisions. The values of CAP for these and other collision pairs are listed in Table 1, along with the VHS diameter d and exponent η, as well as the Morse parameter α. Note that the listed CAP values are obtained for the VHS model, and they may be used with the VSS model. As mentioned previously, the CAP is the correction to the total collision cross section, and thus depends on the molecular interaction parameters and not the vibrational energy transfer model. The use of the FHO-FR with other interaction models, such as the inverse-power law or Lennard–Jones, is generally possible but would require the corresponding modification of the first term in Eq. (6) and the CAP.

V. Comparison of FHO and FHO-FR Models

The implementation of the 3-D FHO-FR model is marginally more complex than that of the 1-D FHO model, and therefore

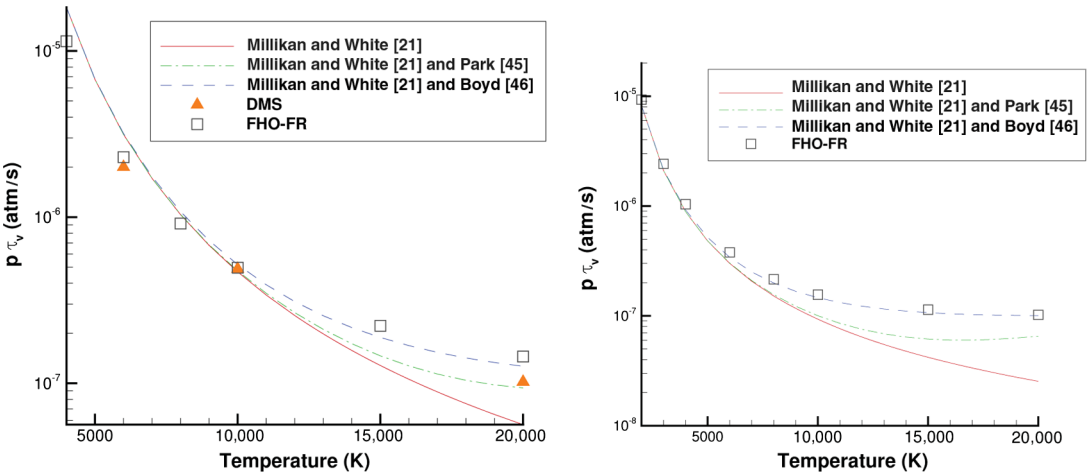

Fig. 4 Relaxation times for N_2–N_2 (left) and O_2–O_2 (right).

recommended due to its higher accuracy. The extensive use of the 1-D FHO model in the past, however, and its implementation in a number of codes still raises the question of the amount of difference between the gas properties obtained by the FHO and the FHO-FR models. The following results provide some insight into this.

The 1-D FHO model uses a steric factor to adjust its transition probabilities, which lack the dependence on the orientation of the colliders, to match some known values, either at the microscopic energy-dependent or macroscopic temperature-dependent level. The availability of FHO-FR probabilities, which explicitly include such a dependence, and thus do not use a steric factor, makes the adjustment procedure fairly straightforward. The use of steric factors of 1/70 for O_2 and 1/14 for N_2 provides good agreement between the FHO and FHO-FR for low and moderate energies up to those of the corresponding probability maximums of the FHO. The comparison of different energy-dependent deexcitation probabilities for the FHO and FHO-FR is shown in Fig. 5 (left) for O_2–O_2 collisions. The total collision energy represents the sum of the relative translational and rotational modes, and it is normalized by the Boltzmann constant. From the numbers of degrees of freedom in different modes, one can estimate that the gas temperatures are approximately two times lower than the corresponding normalized collision energies. As expected, all FHO probabilities peak out at some energies, and they sharply decrease after that.

Comparison of the FHO and FHO-FR probabilities indicates that there is little difference in low vibrational level transitions until the gas temperatures exceed 10,000 K; after which, FHO probabilities start to decrease. The difference for higher levels becomes pronounced at significantly lower temperatures. However, the population of these higher levels at low temperatures is fairly small, and their impact should therefore be limited. The results for N_2–N_2 (not shown here) are similar, with the main difference being the shift of probability curves toward higher temperatures due to larger vibrational energy quanta (for example, the $1 \rightarrow 0$ FHO probability peaks at almost 100,000 K for N_2 as compared to less than 40,000 K for O_2). Because the impact of the FHO vs FHO-FR difference is expected at much lower temperatures for O_2 than for N_2, only oxygen is considered here.

A comparison of temperature-dependent vibrational relaxation times for the two VT models is presented in Fig. 5 (right). There is an excellent agreement for temperatures up to 5000 K, where the VT relaxation is governed mostly by single-quantum transitions between low vibrational levels. At higher temperatures, the impact of 1-D approximation becomes visible. At 10,000 K, the FHO model has two times slower VT relaxation rate as compared to the FHO-FR. At even higher temperatures, where higher vibrational levels become dominant contributors to the total vibrational energy, the relaxation time starts to increase for the FHO model and, at 20,000 K, the difference exceeds one order of magnitude. At flow conditions where the gas temperature exceeds 10,000 K, the FHO model may therefore be expected to significantly underpredict the VT relaxation rate. Although this is a very large difference that should not be neglected, it is also important to project it to real high-temperature gas flows, where competing processes such as molecular dissociation and atom–molecule collisions play significant roles.

Table 1 VHS/VSS and FHO-FR parameters for different interaction types

Pair	d, Å	η	α, Å^{-1}	CAP
N_2–N_2	4.467	0.25	3.7	5.0
N_2–O_2	4.226	0.23	4.0	4.0
O_2–N_2	4.226	0.23	4.0	4.0
O_2–O_2	3.985	0.21	4.0	3.0
O_2–Ar	4.078	0.25	4.0	1.33

To this end, a two-dimensional supersonic flow of molecular oxygen over a plate placed perpendicular to the flow is modeled. The general flow setup is similar to that of [23]: the gas pressure and temperature are 0.8 torr and 295 K, respectively; pure O_2 is in the freestream; there is a low Knudsen number of 2×10^{-4}, which allows one to obtain a 1-D normal shock profile along the stagnation streamline; there is specular reflection at the wall; and there is a total of about 200 million particles and 7 million cells, which are sufficient to provide molecule- and cell-independent results. To examine the impact of the VT model in different temperature regimes, two flow velocities are considered: 4.44 and 6.66 km/s. The bias dissociation model [16,47] is used in these calculations, and the Larsen–Borgnakke model is used to simulate the rotation–translation energy transfer, as well as to simulate the vibration–translation transfer in O_2–O collisions. The temperature-dependent VT rate of [48] is used for the latter.

Gas translational and vibrational temperatures and atomic oxygen mole fraction X[O] along the stagnation streamline are shown in Fig. 6 (left) for the 4.44 km/s case. Note that the plate is at a distance of 4 cm, and the plot shows zoomed-in details of the nonequilibrium shock front. A higher VT relaxation rate in the FHO-FR model results in a more rapid increase of the vibrational temperature as compared to the FHO and somewhat lower translational temperatures due to faster vibration-to-translation energy transfer. The difference in vibrational temperature inside the shock front amounts to approximately 20%. Faster vibrational relaxation for the FHO-FR causes more dissociation reactions due to its high vibrational favoring, which in turns results in larger atomic oxygen mole fraction throughout the shock. More dissociation reactions are the reason for approximately a 60 K lower maximum vibrational temperature for the FHO-FR model.

The higher freestream velocity case of 6.66 km/s is shown in Fig. 6 (right). For this high-velocity case, the translational temperature is much higher, reaching almost 25,000 K at its peak. Still, the difference between the vibrational temperatures obtained using the FHO and FHO-FR models is about 20% in the shock front,

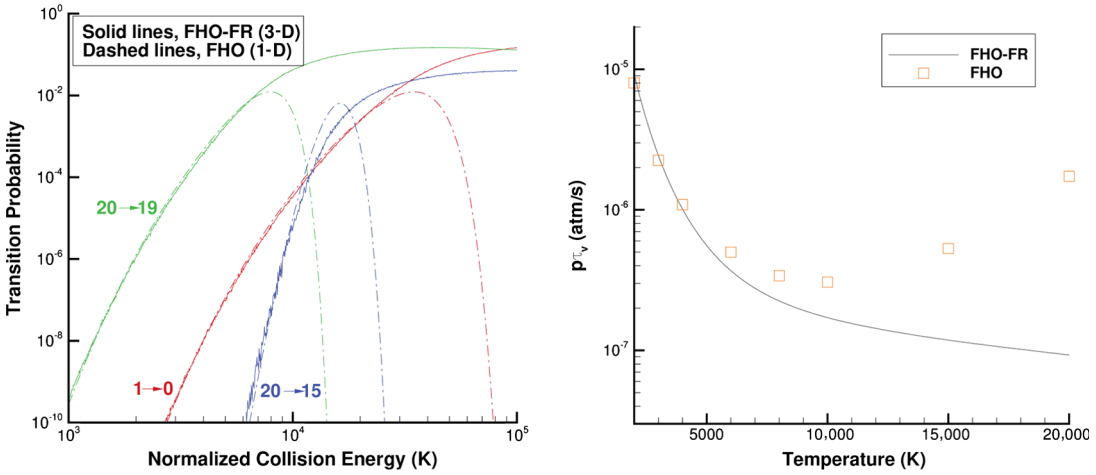

Fig. 5 Comparison of FHO-FR and FHO VT transition probabilities (left) and relaxation times (right) for molecular oxygen.

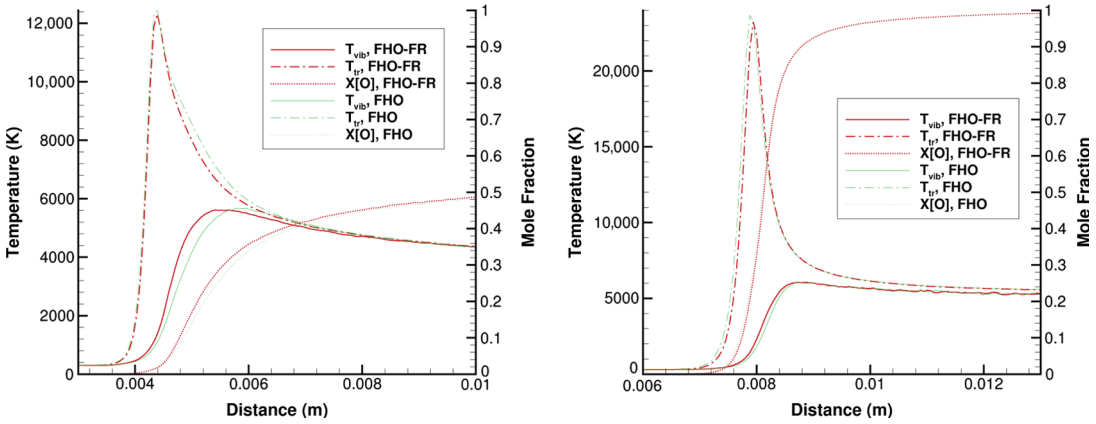

Fig. 6 Flow properties along the stagnation streamline in reacting oxygen for two VT models and flow velocities of 4.44 km/s (left) and 6.66 km/s (right).

which is similar to the low-velocity case. Moreover, there is almost no difference downstream from the peak of vibrational temperature. Such a moderate impact of the VT model (compare this to the difference in vibrational relaxation time; see Fig. 5) is explained by the dissociation of molecular oxygen in the high-temperature shock: the oxygen is mostly dissociated, even before the vibrational temperature reaches its peak. Because of that, the vibrational relaxation of O_2 mostly proceeds through its collisions with atomic oxygen, which is up to an order of magnitude faster than that of O_2–O_2. Note that the lower translational temperature and atomic oxygen mole fraction inside the shock for the FHO-FR model are associated with a reduced standoff distance, caused by faster VT relaxation and dissociation. For both VT models, the vibrational and translational temperatures after the shock converge very slowly, with the vibrational temperature being several hundred degrees lower, due to the depletion of high vibrational states as a result of the vibration–dissociation coupling.

Although the impact of the 1-D FHO approximation in pure oxygen is moderate, it significantly increases when oxygen concentration is relatively small. An example is presented in Fig. 7, where the flow properties are shown for hypersonic flow of Ar–O_2, which is the gas mixture often studied in shock tubes (see, for example, [49]). The freestream is an 80% Ar–20% O_2 mixture with a pressure of 0.8 torr, a temperature of 295 K, and a velocity of 3 km/s. It is seen in Fig. 7 that the standoff distance is noticeably smaller for the 3-D FHO model, and the vibrational excitation is over two times faster. The aftershock relaxation also differs, with a larger impact of dissociation and a larger difference between translational and vibrational temperatures for the FHO-FR model. Note that the translational and vibrational temperatures do not equilibrate due to the depletion of high vibrational levels (a quasi-steady state; see, for

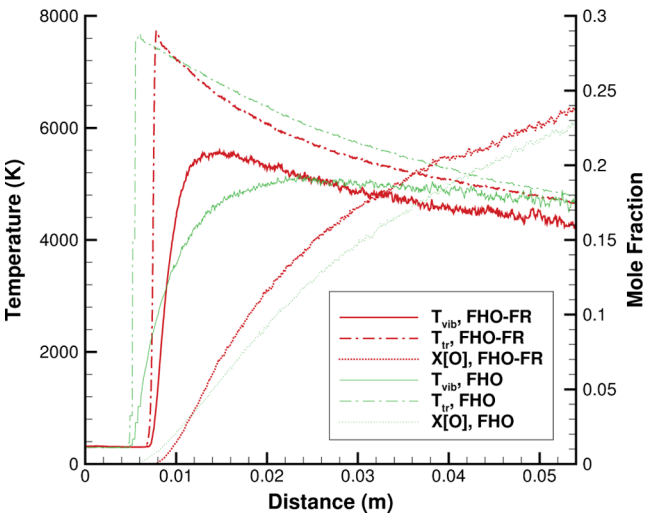

Fig. 7 Properties along the stagnation streamline for an O_2–Ar flow at 3 km/s.

example, [10]). The difference in vibrational temperatures of oxygen diluted in argon, obtained by the 1-D FHO and FHO-FR, further increases with flow velocity, although higher shock front temperatures result in fast dissociation of O_2. For example, in a 4.44 km/s flow of 80% Ar–20% O_2 (not shown here), by the time oxygen dissociates in the shock front, its vibrational temperature reaches over 6000 K according to the FHO-FR model but only 4500 K for the 1-D FHO. The impact of the 1-D assumption in the

FHO model on the oxygen properties is expected to be nearly as large for air because the dissociation threshold for nitrogen is much higher than for oxygen, resulting in higher aftershock temperatures in air as compared to pure oxygen.

VI. Conclusions

This work presents the first adaptation of the three-dimensional FHO-FR model for the DSMC method, which is focused on the vibration–translation energy transfer in atom–diatom and diatom–diatom collisions. The proposed algorithm is computationally efficient because it uses lookup tables of energy-dependent transition probabilities that are calculated before DSMC simulations. It employs the microscopic reversibility condition to calculate deexcitation probabilities from the corresponding excitation processes, and it satisfies the detailed balance requirement for equilibrium conditions. It does not use the energy symmetrization assumption that many one-dimensional FHO model implementations rely upon. A cross-section adjustment parameter is introduced that allows direct use of the FHO-FR probabilities in DSMC simulations with the VHS and VSS molecular interaction models. Note that the proposed algorithm is flexible enough to be used along with other elastic collision models, requiring minimum modifications for that.

The present implementation is verified in adiabatic and isothermal heat bath conditions, and it is shown to reach and maintain equilibrium at micro- and macroscopic levels. Collisions of molecular species of air are considered, and the CAPs for these collisions are obtained that allow matching of the known temperature-dependent vibrational relaxation rates. The validation is conducted for an aftershock recombination of atomic oxygen in argon, and good agreement with available experimental data is observed. Note that the simplicity of implementation of the FHO-FR model, its accuracy in modeling energy transfer in nonreactive collisions, and its high numerical efficiency and low computational cost make it an attractive choice for modeling multidimensional rarefied flows. Moreover, the model is general enough to include, using the same framework, collisions of most species of interest.

A comparison of 1-D and 3-D FHO models is performed at the level of energy-dependent VT probabilities, temperature-dependent vibrational relaxation time, and hypersonic flow of dissociating oxygen. Large differences are observed in oxygen vibrational relaxation times at high temperatures, with the 1-D FHO relaxation time overpredicting the 3-D FHO by over an order of magnitude at 20,000 K. The difference is much smaller, at less than a factor of two, for nitrogen due to larger vibrational quanta and lower VT probabilities at these temperatures. The difference in vibrational temperatures of hypersonic dissociating oxygen for 1-D and 3-D FHOs is moderate; on average, it is about 20% for flow velocities between 4 and 7 km/s. That difference is expected to significantly increase in gas mixtures with low to moderate concentrations of oxygen, such as air flows or oxygen diluted in noble gases. This is primarily due to the dominant effect of nonoxygen species with lower dissociation rates, which should result in higher gas temperatures as compared to dissociating oxygen flows.

Acknowledgments

The work was supported in part by the U.S. Air Force Office of Scientific Research (Program Officer Ivett Leyva). Computational support from The Extreme Science and Engineering Discovery Environment (XSEDE) (grant OCI-1053575) and High Performance Computing Modernization Program (HPCMP) (project AFPRD04682021) is appreciated.

References

[1] Bird, G. A., *Molecular Gas Dynamics and the Direct Simulation of Gas Flows*, Clarendon, Oxford, England, U.K., 1994, pp. 99–147.

[2] Ivanov, M. S., and Gimelshein, S. F., "Computational Hypersonic Rarefied Flows," *Annual Review of Fluid Mechanics*, Vol. 30, No. 1, 1998, pp. 469–505.
doi:10.1146/annurev.fluid.30.1.469

[3] Gorbachev, Yu. E., and Mallinger, F., "Quasi-Classical Model for Vibrational—Translational and Vibrational—Vibrational Rate Constants," *Journal of Thermophysics and Heat Transfer*, Vol. 13, No. 4, 1999, pp. 411–423.
doi:10.2514/2.6475

[4] Esposito, F., Capitelli, M., and Gorse, C., "Quasi-Classical Dynamics and Vibrational Kinetics of $N + N_2(V)$ System," *Chemical Physics*, Vol. 257, No. 2, 2000, pp. 193–202.
doi:10.1016/S0301-0104(00)00155-5

[5] Varandas, A. J. C., and Marques, J. M. C., "Method for Quasiclassical Trajectory Calculations on Potential Energy Surfaces Defined from Gradients and Hessians, and Model to Constrain the Energy in Vibrational Modes," *Journal of Chemical Physics*, Vol. 100, No. 3, 1994, pp. 1908–1920.
doi:10.1063/1.466544

[6] Billing, G., and Fisher, E., "VV and VT Rate Coefficients in N_2 by a Quantum-Classical Model," *Chemical Physics*, Vol. 43, No. 3, 1979, pp. 395–401.
doi:10.1016/0301-0104(79)85207-6

[7] Billing, G., *The Quantum Classical Theory*, Oxford Univ. Press, New York, 2003, pp. 57–71.

[8] Chapuisat, X., and Bergeron, G., "Anharmonicity Effects in the Collinear Collision of Two Diatomic Molecules," *Chemical Physics*," Vol. 36, No. 3, 1979, pp. 397–405.
doi:10.1016/0301-0104(79)85023-5

[9] Li, Z., Parsons, N., and Levin, D. A., "A Study of Internal Energy Relaxation in Shocks Using Molecular Dynamics Based Models," *Journal of Chemical Physics*, Vol. 143, Oct. 2015, Paper 144501.

[10] Valentini, P., Schwartzentruber, T. E., Bender, J. D., Nompelis, I., and Candler, G. V., "Direct Molecular Simulation of Nitrogen Dissociation Based on an *ab initio* Potential Energy Surface," *Physics of Fluids*, Vol. 27, No. 8, 2015, Paper 086102.
doi:10.1063/1.4929394

[11] Panesi, M., Jaffe, R. L., Schwenke, D. W., and Magin, T. E., "Rovibrational Internal Energy Transfer and Dissociation of N_2–N System in Hypersonic Flows," *Journal of Chemical Physics*, Vol. 138, No. 4, 2013, Paper 044312.
doi:10.1063/1.4774412

[12] Guy, A., Bourdon, A., and Perrin, M.-Y., "Derivation of a Consistent Multi-Internal-Temperature Model for Vibrational Energy Excitation and Dissociation of Molecular Nitrogen in Hypersonic Flows," AIAA Paper 2013-0194, 2013.

[13] Esposito, F., Armenise, I., Capitta, G., and Capitelli, M., "O–O_2 State-to-State Vibrational Relaxation and Dissociation Rates Based on Quasiclassical Calculations," *Chemical Physics*, Vol. 351, Nos. 1–3, 2008, pp. 91–98.
doi:10.1016/j.chemphys.2008.04.004

[14] Andrienko, D., and Boyd, I. D., "Master Equation Study of Vibrational and Rotational Relaxations of Oxygen," *Journal of Thermophysics and Heat Transfer*, Vol. 30, No. 3, 2016, pp. 533–552.
doi:10.2514/1.T4769

[15] Valentini, P., Norman, P., Zhang, C., and Schwartzentruber, T. E., "Rovibrational Coupling in Molecular Nitrogen at High Temperature: An Atomic-Level Study," *Physics of Fluids*, Vol. 26, No. 5, 2014, Paper 056103.
doi:10.1063/1.4875279

[16] Koura, K., "A Set of Model Cross Sections for the Monte Carlo Simulation of Rarefied Real Gases: Atom–Diatom Collisions," *Physics of Fluids*, Vol. 6, No. 10, 1994, pp. 3473–3486.
doi:10.1063/1.868404

[17] Koura, K., "Monte Carlo Direct Simulation of Rotational Relaxation of Diatomic Molecules Using Classical Trajectory Calculations: Nitrogen Shock Wave," *Physics of Fluids*, Vol. 9, No. 11, 1997, pp. 3543–3549.
doi:10.1063/1.869462

[18] Adamovich, I. V., "Three-Dimensional Analytic Probabilities of Coupled Vibrational-Rotational-Translational Energy Transfer for DSMC Modeling of Nonequilibrium Flows," *Physics of Fluids*, Vol. 26, No. 4, 2014, Paper 046102.
doi:10.1063/1.4872336

[19] Borgnakke, C., and Larsen, P. S., "Statistical Collision Model for Monte Carlo Simulation of Polyatomic Gas Mixture," *Journal of Computational Physics*, Vol. 18, No. 4, 1975, pp. 405–420.
doi:10.1016/0021-9991(75)90094-7

[20] Bergemann, F., and Boyd, I. D., "DSMC Simulation of Inelastic Collisions Using the Borgnakke-Larsen Method Extended to Discrete Distributions of Vibrational Energy," *Rarefied Gas Dynamics: Theory and Simulations*, Vol. 158, Progress in Astronautics and Aeronautics, edited by B. D. Shizgal, and D. P. Weaver, AIAA, Washington, D.C., 1994, pp. 174–183.

[21] Millikan, R. C., and White, D. R., "Systematics of Vibrational Relaxation," *Journal of Chemical Physics*, Vol. 39, No. 12, 1963, pp. 3209–3213. doi:10.1063/1.1734182

[22] Gimelshein, S. F., Ivanov, M. S., Markelov, G. N., and Gorbachev, Yu. E., "Statistical Simulation of Nonequilibrium Rarefied Flows with Quasiclassical Vibrational Energy Transfer Models," *Journal of Thermophysics and Heat Transfer*, Vol. 12, No. 4, 1998, pp. 489–495. doi:10.2514/2.6394

[23] Wysong, I., Gimelshein, S., Bondar, Y., and Ivanov, M., "Comparison of DSMC Chemistry and Vibrational Models Applied to Oxygen Shock Measurements," *Physics of Fluids*, Vol. 26, No. 4, 2014, Paper 043101. doi:10.1063/1.4871023

[24] Munafo, A., Panesi, M., and Magin, T. E., "Boltzmann Rovibrational Collisional Model for Internal Energy Excitation and Dissociation in Hypersonic Flows," *Physical Review E*, Vol. 89, No. 2, 2014, Paper 023001. doi:10.1103/PhysRevE.89.023001

[25] Schwartz, R., Slawsky, Z., and Herzfeld, K., "Calculation of Vibrational Relaxation Times in Gases," *Journal of Chemical Physics*, Vol. 20, No. 10, 1952, pp. 1591–1599. doi:10.1063/1.1700221

[26] Kerner, E. H., "Note on the Forced and Damped Oscillator in Quantum Mechanics," *Canadian Journal of Physics*, Vol. 36, No. 3, 1958, pp. 371–377. doi:10.1139/p58-038

[27] Zelechow, A., and Rapp, D., "Vibrational-Vibrational-Translational Energy Transfer Between Two Diatomic Molecules," *Journal of Chemical Physics*, Vol. 49, No. 1, 1968, pp. 286–299. doi:10.1063/1.1669823

[28] Kamimoto, G., and Matsui, H., "Vibrational Energy Exchange on N_2–O_2 Collision," *AIAA Journal*, Vol. 7, No. 12, 1969, pp. 2358–2360. doi:10.2514/3.5551

[29] Adamovich, I., Macheret, S., Rich, J., and Treanor, C., "Vibrational Relaxation and Dissociation Behind Shock Waves Part 1: Kinetic Rate Models," *AIAA Journal*, Vol. 33, No. 6, 1995, pp. 1064–1069. doi:10.2514/3.12528

[30] Boyd, I. D., and Josyula, E., "State Resolved Vibrational Relaxation Modeling for Strongly Nonequilibrium Flows," *Physics of Fluids*, Vol. 23, No. 5, 2011, Paper 057101. doi:10.1063/1.3584128

[31] Li, Z., Zhu, T., and Levin, D. A., "DSMC Simulation of Vibrational Excitation and Reaction for Molecular Nitrogen in Shock Tube Flows," AIAA Paper 2013-1201, 2013.

[32] Weaver, A., Ayyaswamy, V., and Alexeenko, A., "Implementation Challenges and Performance of Forced Harmonic Oscillator Model in DSMC," AIAA Paper 2013-2783, 2013.

[33] Liechty, D. S., "State-to-State Internal Energy Relaxation Following the Quantum-Kinetic Model in DSMC," AIAA Paper 2013-2901, 2013.

[34] Deschenes, T. R., Braunstein, M., and Boyd, I. D., "Comparison of Vibrational Relaxation Modeling for Strongly Non-Equilibrium Flows," AIAA Paper 2014-1076, 2014.

[35] Adamovich, I. V., and Rich, J. W., "Three-Dimensional Nonperturbative Analytic Model of Vibrational Energy Transfer in Atom-Molecule Collisions," *Journal of Chemical Physics*, Vol. 109, No. 18, 1998, 7711–7724. doi:10.1063/1.477417

[36] Adamovich, I. V., "Three-Dimensional Model of Vibrational Energy Transfer in Molecule-Molecule Collisions," *AIAA Journal*, Vol. 39, No. 10, 2001, pp. 1916–1925. doi:10.2514/2.1181

[37] Koura, K., and Matsumoto, H., "Variable Soft Sphere Molecular Model for Inverse-Power-Law or Lennard–Jones Potential," *Physics of Fluids A*, Vol. 3, No. 10, 1991, pp. 2459–2465. doi:10.1063/1.858184

[38] Josyula, E., Suchyta, C. J., Vogiatzis, K., and Vedula, P., "State-to-State Kinetic Modeling of Select Air Species in Hypersonic Nonequilibrium Flows," AIAA Paper 2017-3489, 2017.

[39] Mahan, B. H., "Microscopic Reversibility and Detailed Balance," *Journal of Chemical Education*, Vol. 52, No. 5, 1975, pp. 299–302. doi:10.1021/ed052p299

[40] Ivanov, M. S., Markelov, G. N., and Gimelshein, S. F., "Statistical Simulation of the Transition Between Regular and Mach Reflection in Steady Flows," *Computers and Mathematics with Applications*, Vol. 35, Nos. 1–2, 1998, pp. 113–125. doi:10.1016/S0898-1221(97)00262-9

[41] Kim, J. G., and Boyd, I. D., "Monte Carlo Simulation of Nitrogen Dissociation Based on State-Resolved Cross Sections," *Physics of Fluids*, Vol. 26, Jan. 2014, Paper 012006.

[42] Wray, K. L., "Shock-Tube Study of the Recombination of O Atoms by Ar Catalysts at High Temperatures," *Journal of Chemical Physics*, Vol. 38, No. 7, 1963, pp. 1518–1524. doi:10.1063/1.1776912

[43] Gimelshein, S. F., and Wysong, I. J., "DSMC Modeling of Flows with Recombination Reactions," *Physics of Fluids*, Vol. 29, No. 6, 2017, Paper 067106. doi:10.1063/1.4986529

[44] Andrienko, D. A., and Boyd, I. D., "Simulation of O_2–N Collisions on *ab-initio* Potential Energy Surfaces," AIAA Paper 2016-1249, 2016.

[45] Park, C., "Problems of Rate Chemistry in the Flight Regimes of Aeroassisted Orbital Transfer Vehicles," *Thermal Design of Aeroassisted Orbital Transfer Vehicles*, Progress in Astronautics and Aeronautics, Vol. 6, AIAA, New York, Jan. 1985, pp. 511–537.

[46] Boyd, I. D., "Analysis of Vibration–Dissociation–Recombination Processes Behind Strong Shock Waves of Nitrogen," *Physics of Fluids A*, Vol. 4, No. 1, 1992, pp. 178–185. doi:10.1063/1.858495

[47] Wadsworth, D., and Wysong, I., "Vibrational Favoring Effect in DSMC Dissociation Models," *Physics of Fluids A*, Vol. 9, No. 12, 1997, pp. 3873–3884. doi:10.1063/1.869487

[48] Kulakhmetov, M., Gallis, M., and Alexeenko, A., "Ab Initio-Informed Maximum Entropy Modeling of Rovibrational Relaxation and State-Specific Dissociation with Application to the O_2 + O System," *Journal of Chemical Physics*, Vol. 144, No. 17, 2016, Paper 174302. doi:10.1063/1.4947590

[49] Owen, K. G., Davidson, D. F., and Hanson, R. K., "Oxygen Vibrational Relaxation Times: Shock Tube/Laser Absorption Measurements," *Journal of Thermophysics and Heat Transfer*, Vol. 30, No. 4, 2016, pp. 791–798. doi:10.2514/1.T4505